J. KAU: Earth Sci., **vol. 5**, pp. 1-21 (1412 A.H./1992 A.D.)

Analysis of Fracture Pattern in the Jabal Al-Hassir Ring Complex, Central Arabian Shield

M.A. ALWASHI and S.R. DIVI
Faculty of Earth Sciences, King Abdulaziz University, Jeddah, Saudi Arabia

ABSTRACT. Fractures are delineated from the enhanced Landsat Image and aerial photographs of the Jabal Al-Hassir ring complex area in the Central Arabian Shield. These fractures are validated by field study and measurements. The delineated fractures and interpreted faults are statistically analyzed by "rose diagram" in terms of number, total length and average length of fractures per directional class. Fracture pattern in the elliptical ring complex are compared with those for the country rocks, and discrepancies are suggested to be due to the difference in the tectonic history between the ring complex and the country rocks.

Introduction

Location

The study area is located in the southeastern part of the Precambrian Arabian Shield (Fig. 1). It can be accessed from the town of Bisha by the main desert track to the village of Tathlith.

Bisha is well connected to Jeddah by paved highway and by air transport.

Regional Geology of the Arabian Shield

The Arabian Shield consists of Upper Proterozoic layered sequences, which include metamorphosed mafic to felsic volcanic, volcanoclastic and sedimentary rocks, and plutons that range in composition from ultramafic to felsic. The stratigraphy of the layered sequences is not clearly understood, although they have been subdivided into a number of groups (see Johnson and Vranas 1984 for a comprehensive review). These layered sequences have been repeatedly intruded by various types of plutonic rocks. Based mainly on radiometric ages for these intrusive rocks, orogenic events

for the Shield have been suggested (Johnson and Vranas 1984, Drysdall *et al.* 1985). The layered sequence has commonly been metamorphosed to the amphibolite facies grade and, because of intense deformation, the contact relations of some of the felsic orthogneisses have become almost conformable.

Accordingly this gave rise to the suggestions that the gneisses may represent a possible sialic basement to the layered sequences (Coleman 1972) in addition, although this has not been resolved by dating. However, radiometric ages of the layered sequences and their intrusive rocks generally lie in the range of 900-600 Ma, but there are

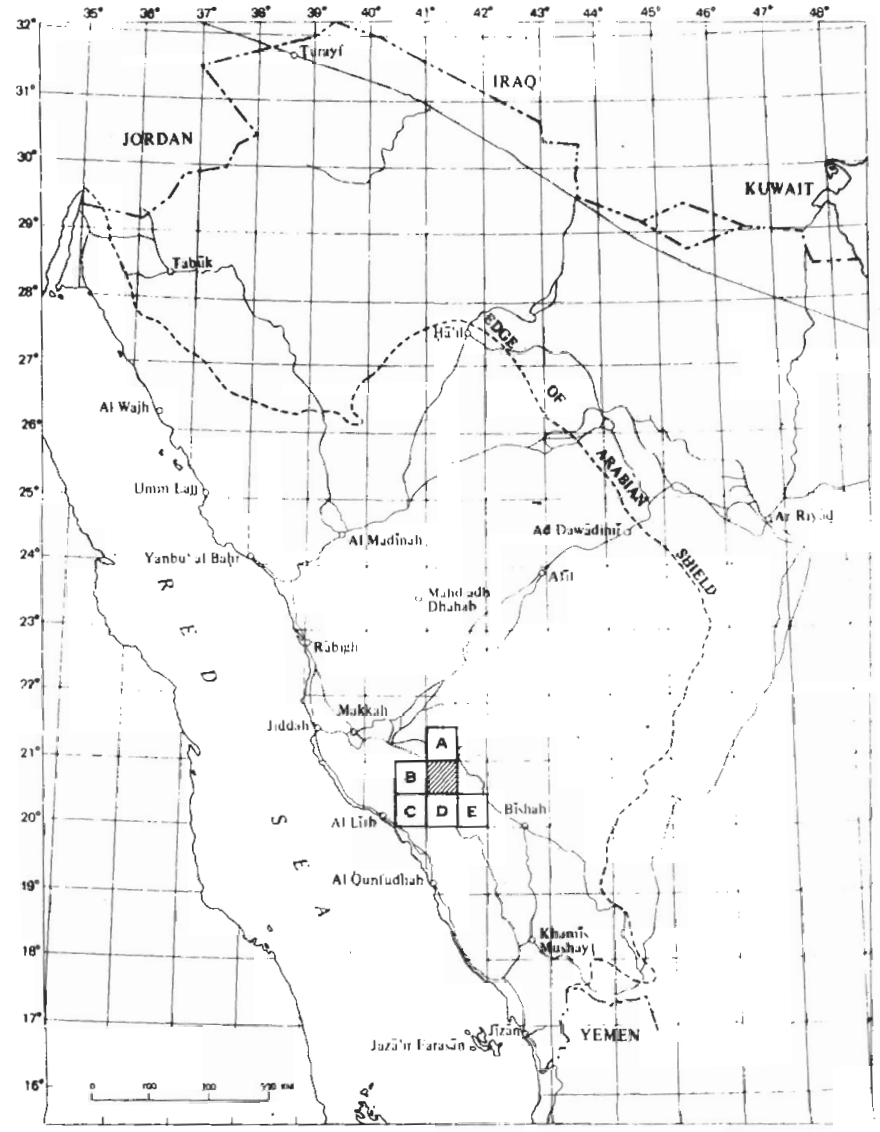

FIG. 1. Location map of the study area (marked as shaded square dots).

rare instances of older ages, upto 2000 Ma (Stacey and Hedge 1984), have given rise to suggestions about an older basement in the Arabian Shield. The general consensus is that the Pan African terrain formed by accretion of microplates composed of intra-oceanic immature island arcs (Johnson and Vranas 1984).

Geology of the Jabal Al-Hassir Area

The dominant geological feature of the oval shaped Jabal Al-Hassir area is the steeply-walled (Pl. 1a) "ring complex". The ring complex is composed of an inner

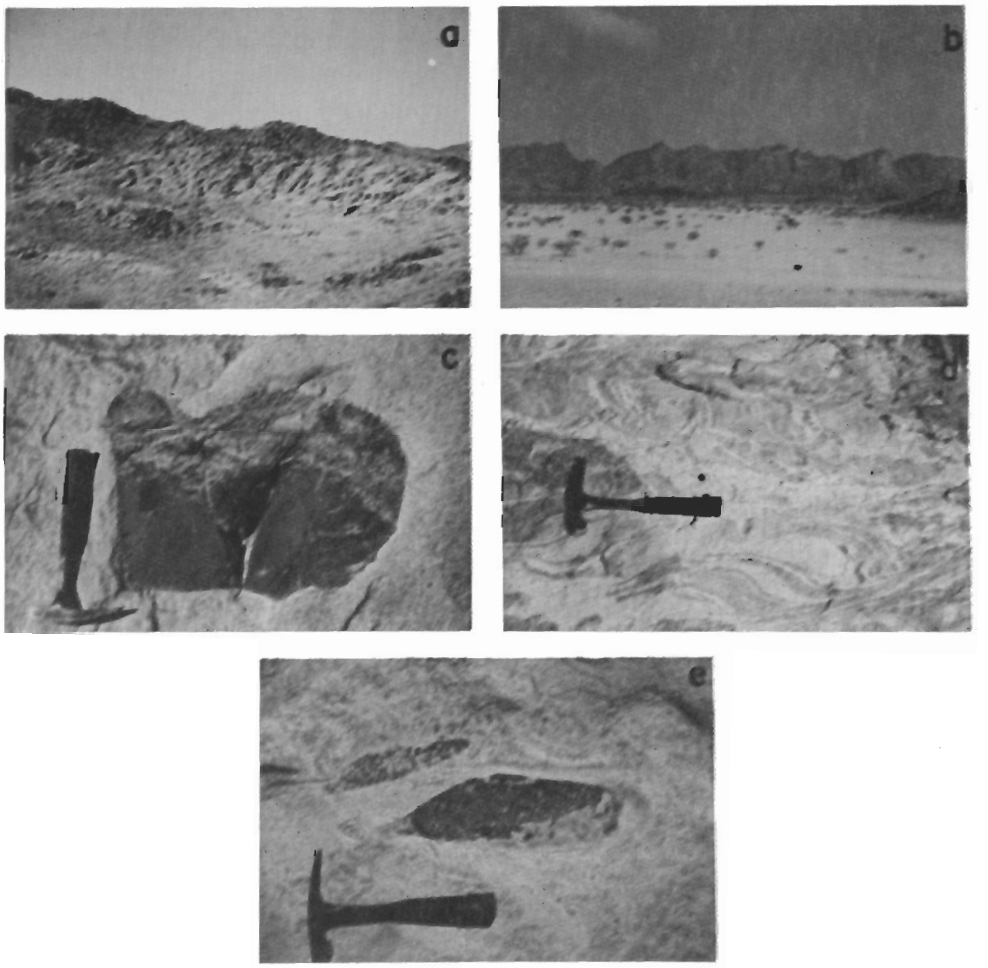

PLATE 1 a. Steep eastern wall of the ridge of the ring complex; note the transverse fractures. The rock is coarse grained pyroxene granite.
b. Dark amphibolite cut by strongly jointed felsic dyke; (field of view approximately 50 meters wide).
c. Migmatitic gneiss composed of leucocratic felsic phase and melanocratic mafic phase.
d. Subangular mafic xenolith in medium grained granitic phase of the ring complex; note the metasomatic replacement of the xenolith in the upper part.
e. Elliptical mafic xenolith in medium grained granitic phase of the ring complex.

zone of biotite granite, and an outer zone of pyroxene granite. The rocks lying outside the complex consist of mafic schists, felsic gneisses and felsic to ultramafic intrusive rocks. The geological map of overstreet (1978) is slightly modified and shown in Fig. 2.

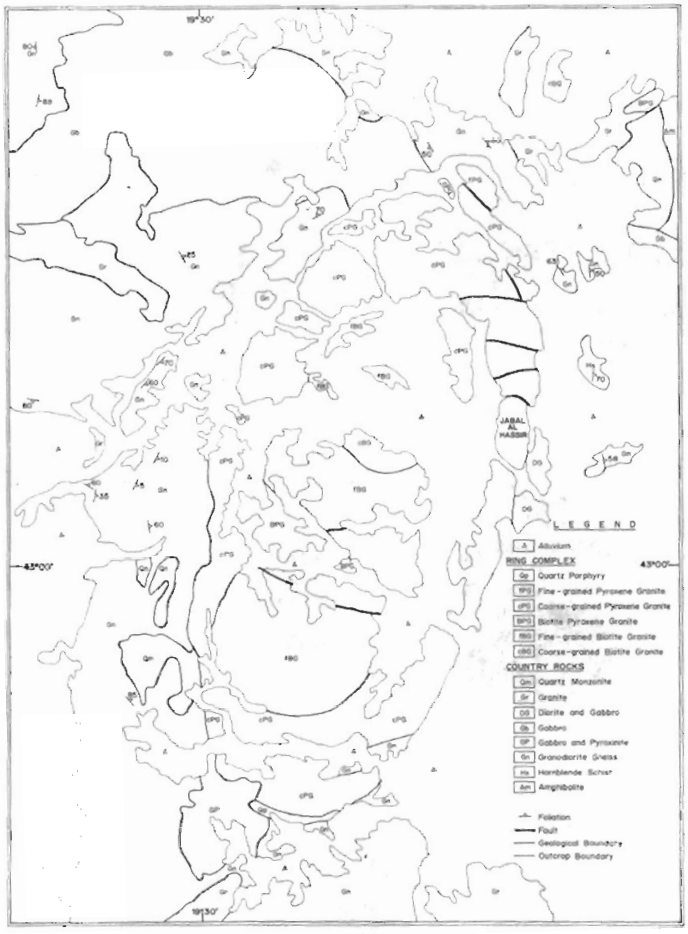

FIG. 2. Geological map of the Jabal Al-Hassir area, slightly modified after overstreet (1978). Map scale is approximately 1:197,000.

The oldest rock in the area are the amphibolite Am (Pl. 1b) and hornblende schist (Am and Hs Fig. 2), which are essentially composed of hornblende and plagioclase. These rocks are medium to fine grained, and dark gray to black in colour. Layering is often visible, but it is difficult to speculate on its origin. Overstreet (1978) considers them to comprise metavolcanics, but they could be deformed layered intrusions. The granodiorite gneiss Gn (Fig. 2) is light gray, medium to coarse grained gneiss consisting of quartz, feldspar, biotite and often hornblende.

Migmatitic features are occasionally observed (Pl. 1c). Xenolithis of mafic schists suggest that the granodiorite gneiss (Gn) is younger than amphibolite (Am) and hornblende schist (Hs). All the three rocks have been complex, particularly in the eastern part of the area, has both concordant (Pl. 2a) and discordant (Pl. 2b) contacts with the country rocks. The implications of this variation will be discussed later.

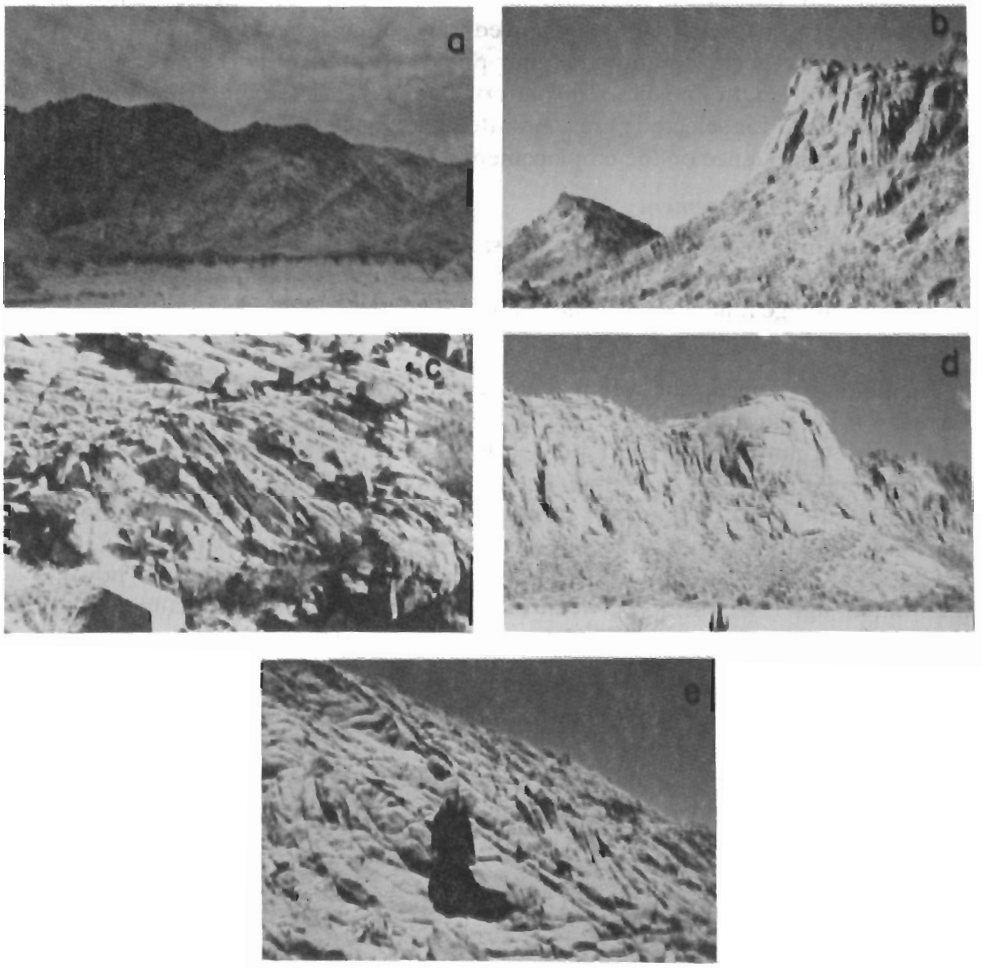

PLATE 2 a. Conformable contact between more resistant granitic ridge of the ring complex to the left and granitic gneiss occupying the lower ground on the right; length of the ridge in the photo approximately 30 meters.

b. Discordant contact between well foilated granitic gneiss on the left and massive granitic outer ridge of the ring complex; field of view approximately 100 meters.

c. Subhorizontal fractures in the granitic outer ridge of the ring complex.

d. Closely spaced minor fracture set cut by a larger subhorizontal fractures; slight splaying of fractures, into the larger fracture could suggest some shearing along the latter.

e. As in Pl. 2d except that the larger fracture set is more dominant than the smaller fracture set.

Purpose and Methods of the Present Study

The present study deals with the delineation of fractures, using aerial photographs and enhanced Landsat images of the ring complex and adjacent surrounding rocks. This study forms part of a larger project that deals with the petrological and structural evolution of the ring complex (Divi *et al.* in preparation). The fracture pattern and its analysis is a pre-requisite to the understanding of the emplacement mechanics of the ring complex. Fractures from the enhanced Landsat images and aerial photographs were delineated, digitized and computer processed to identify the patterns of the orientation and length statistics. The pattern obtained are compared with those measured in the field for selected areas. An attempt is made to interpret the patterns in terms of their influence on the emplacement mechanics of the ring complex.

Landsat Image Enhancement

The study area is covered by the Landsat MSS Scene 179-047. To date, the most successful procedure for the detection of lineaments relies on digital enhancement of the Landsat image followed by visual delineation of the metamorphosed to amphibolite facies grade.

The field relationships between the intrusive plutonic components (Gp, Gb, DG, Gr and Qm) of the country rocks (Fig. 2) are not clear. Their relationships within the ring complex, can be deciphered, but are not as clear outside it. The mafic suite (Gp, Gb, DG) apears to be younger than the ring complex, although in the case of the gabbro-pyroxenite (GP) body, in the southern part of the study area, this relationship may be questioned, based on an apparently discordant outcrop pattern. As regard the felsic suite, the quartz monzonite (Qm) is older than the ring complex; however, the relative age relationship between the granite (Gr) and the ring complex is not clear, because they are not in contact.

The ring complex consists in general of two zones comprising an inner biotite granite and outer pyroxene granite. Further subdivisions are shown in Figure 2, and the complex consists of 6 district rock types (cBG, fBG, cPG, fPG, Qp, BPG) that have an annual pattern in a roughly elleptical body. The outer pyroxene granite (cPG) is pink to red, coarse-grained, and grades inward to central mass of fine-grained biotite granite around a core of coarse grained biotite granite. Occasionally, there is some primary flow banding, defined by segregations of feldspars and pyroxenes. Mafic xenoliths are ubiquitous (Pl. 1-d and e) and are considered to have been derived from the mafic country rocks (Hs, Am). The outer wall of the ring lineaments for the photo-prints of the enhanced image. There are a variety of enhancement procedures, of which four are most commonly used. These are (1) a moving boxcar average, based on the Canada Center for Remote Sensing Image Analysis System (CIAS, Soha *et al.* 1976); (2) a flexible convolution filtering program developed for the ARIES System (Anonymous 1982) capable of enhancing linear features at any selected orientation; using directional first derivative filters; (3) a thresholding algorithm; and (4) a multiple step algorithm somewhat similar to that used by Moore and Waltz (1983) which involves low-pass filtering, directional filtering and addition of the original image.

For the present study, high-pass filtering, contrast enhancement and dodging techniques were applied to band 6 (0.7-0.8 mm) of the image. The digitally enhanced image data were transferred to a photowrite system, from which a print was made (Fig. 3) to visually delineate the lineaments. The delineated fractures (Fig. 4) were digitized for further statistical analysis.

FIG. 3. Landsat image of the Jabal Al-Hassir area. Image Scale is approximately 1:161,000.

Analysis

The lineaments delineated from the enhanced image are shown in Fig. 4, which shows their variability in length and orientation. In general, two preferred orientations of the lineaments are apparent; one approximately NW and the other approximately NE. The longest lineaments have a NW orientation.

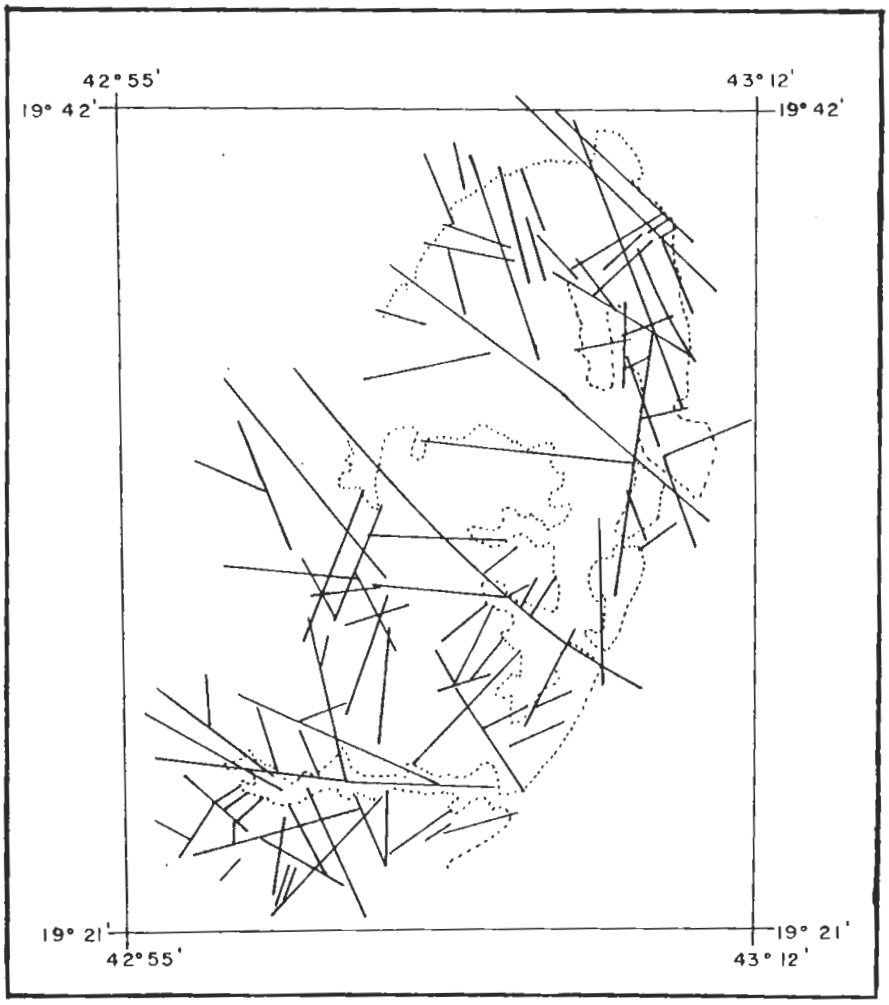

FIG. 4. Fractures delineated from the Landsat image of Jabal Al-Hassir area (Fig. 3); dotted line represents the general outline of the ring complex. Map scale is approximately 1:148,000.

To evaluate and confirm the above visual impressions, the lineaments in Figure 4 were digitized and analysed for their orientation patterns and length distributions.

Figure 5, illustrates these statistics in the form of "rose diagram". The rose diagram in (Fig. 5a) indicates that the lineaments are oriented most frequently in a NNW direction, and to a lesser extent in a ENE direction. The lineaments were the longest lengths are oriented NW and NNW. These features correspond approximately with the visual delineations made on Figure 4, but Figures 5a, 5b, and 5c show that although fractures withan E-W orientation are neither abundant (Fig. 5a) nor of great length (Fig. 5b), their average length is an important feature (Fig. 5c).

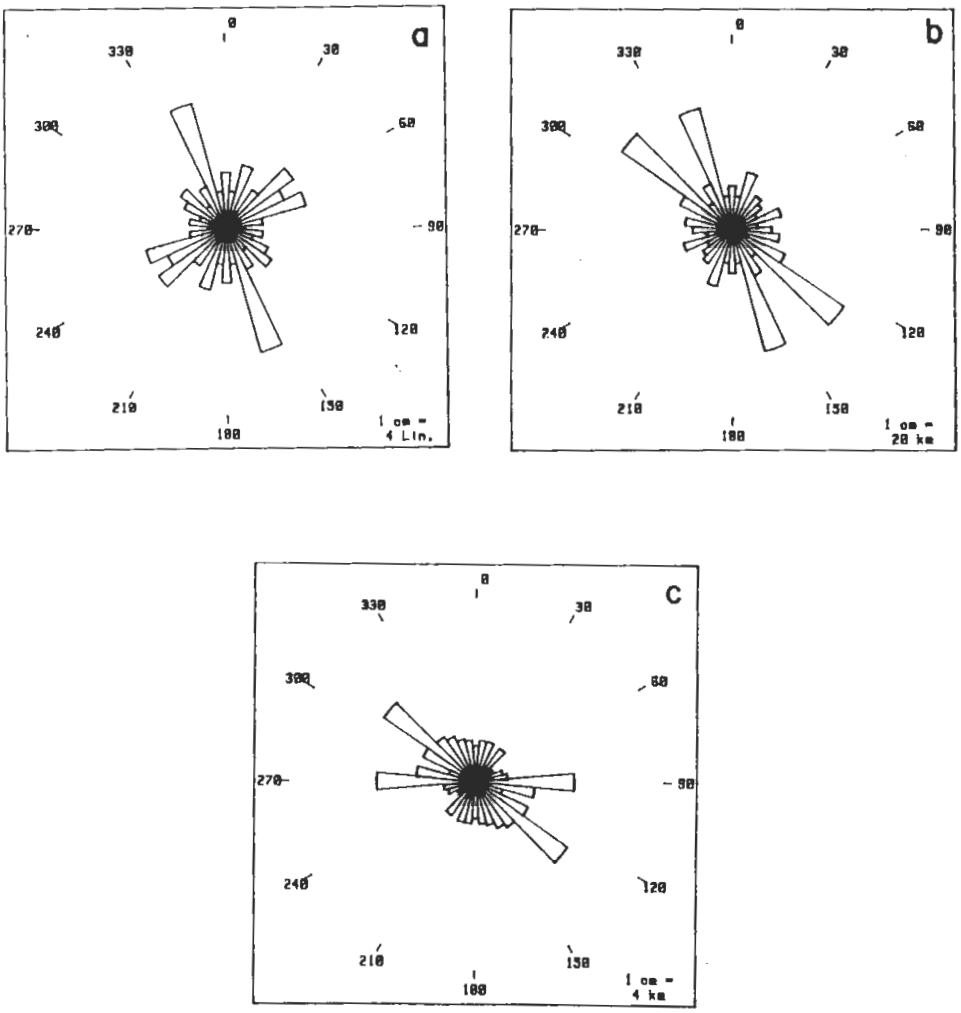

FIG. 5 Rose diagram for fractures delineated from the Landsat image (Fig. 4), 5a – number of fractures, 5b – total length of fractures, 5c – average length of fractures.

Aerial Photos

Photo Preparation and Lineament Delineation

The number of lineaments that can be delineated on aerial photographs is strongly influenced by the scale of the photo. Obviously, very small scale aerial photos link satellite images exhibit only the most dominant lineaments and enlarged photos will display a greater number of lineaments. Therefore, selection of the scale of observation is subjective but is controlled by correspondence with the scale of geological observation (e.g. available geological maps).

For the study area, the prepared geological map is of the scale 1:100,000. To obtain more fracture information, a scale of 1:50,000 was selected for the controlled aerial photo-mosaics. The study area is covered by parts of four mosaics (joined and reduced in Fig. 6). Fractures from these photos were visually delineated and digitized for analysis.

Analysis

(Fig. 7) contains approximately 2500 fracture traces, which exhibit different orientations and spatial extents. The thicker and longer lines are interpreted as major faults. The statistical data on these faults and other fractures are listed respectively. As with the LANDSAT Data (Table 1), these statistics for directional classes are displayed as rose diagrams in Figs. 8 and 9.

The major faults in the area have a general northwesterly trend, and Fig. 7 suggests that they occur in four approximately equally spaced northwest trending zones cutting the elliptical ring complex. Although the significance of this apparent pattern is not clear within the study area, it may be related to a larger scale, regional pattern. Figs. 8a and 8b clearly indicate that the faults are more frequent and extend for longer distances in a northwesterly direction. However, Fig. 8c indicates that the average length of faults is greater in the NNW and W directions.

The smaller fractures in Fig. 7 are more numerous and have variable orientations; there seems to be a slight difference in the pattern of their orientations between the northern and southern parts of the oval ring complex fractures are more variably oriented in the north than in the south, where they are dominantly WNW. However, over the entire area, the dominant WNW direction is clearly apparent, both for the number of fractures (Fig. 9a) and total length of fractures (Fig. 9b), although Fig. 9c, illustrates that the average lengths of fracture in different directional classes are essentially similar.

The lineaments patterns in the area are mainly a result of tectonic stresses. The elliptical shape (Fig. 11) most probably represents an initially circular body deformed by E-W compression. A model for strain analysis of joints was presented by Davis

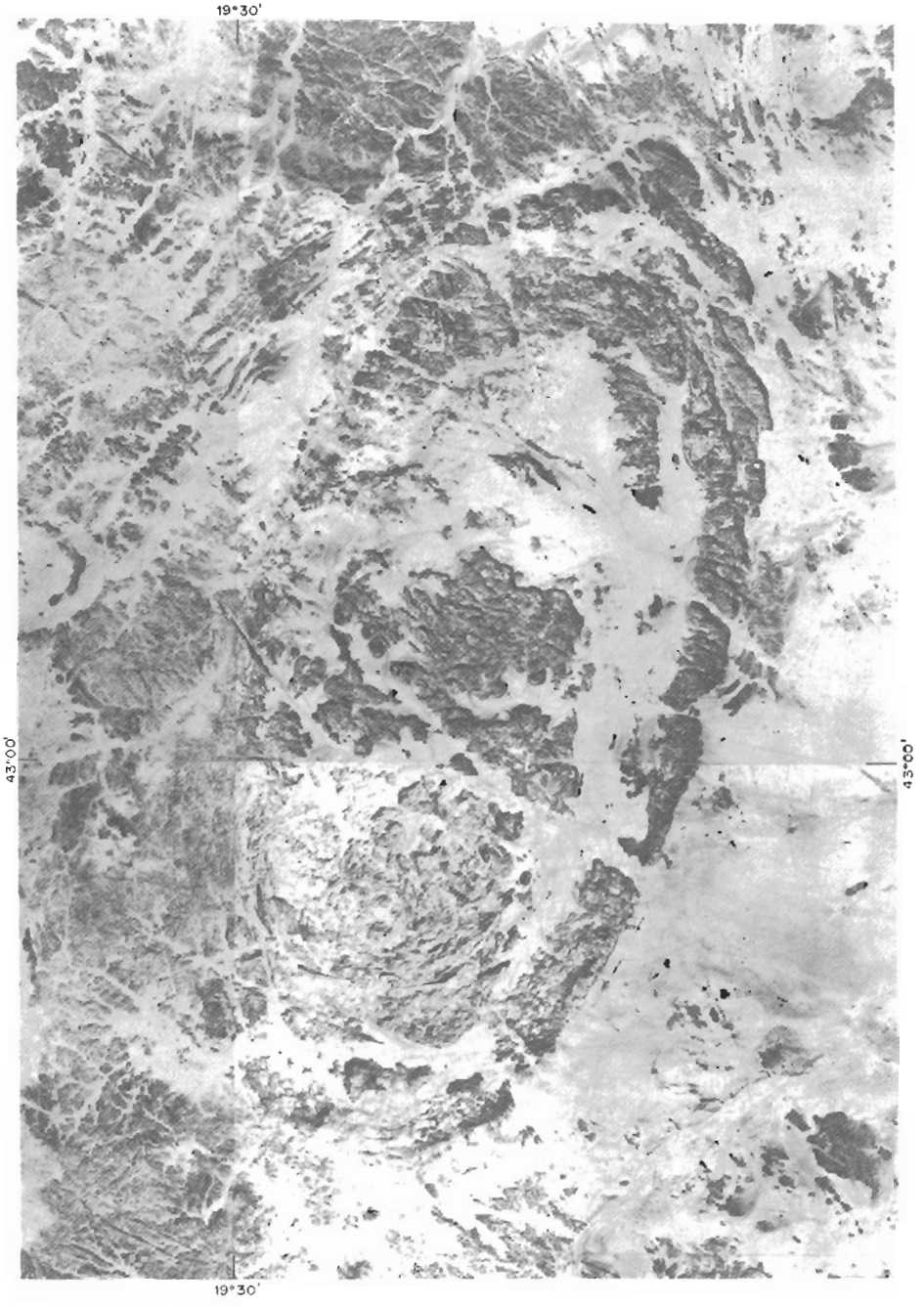

FIG. 6. Aerial Photographs mosaic of the Jabal Al-Hassir area. Photo Scale is approximately 1:158,000.

FIG. 7. Fractures delineated from the aerial photograph of the Jabal Al-Hassir area (Fig. 6). Large fractures could represent faults. Map scale is approximately 1:165,000.

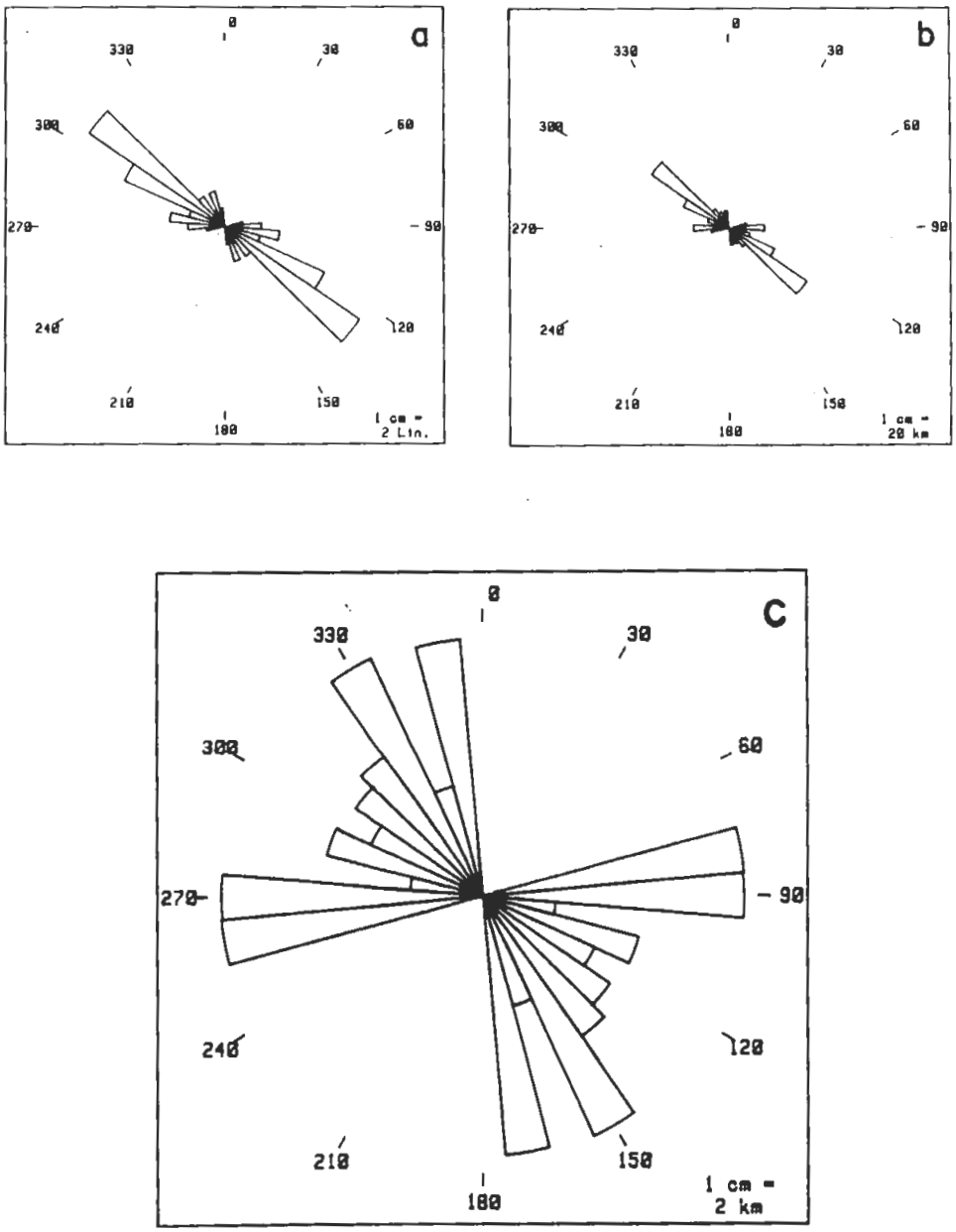

FIG. 8. Rose diagram for faults delineated from the aerial photographs (Fig. 6); 8a – number of faults; 8b – total length of faults; 8c – average length of fractures.

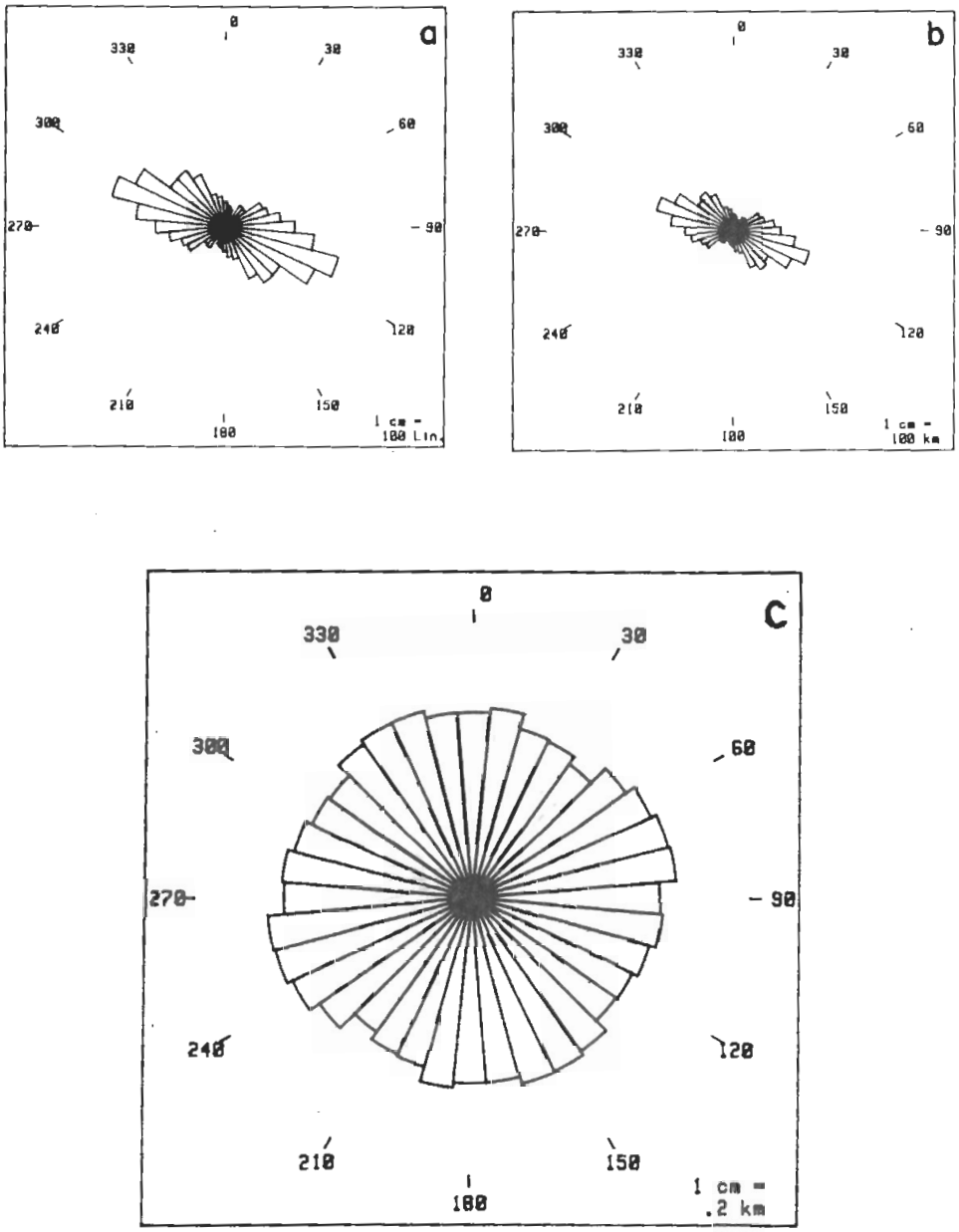

FIG. 9. Rose diagram for smaller fractures delineated from the aerial photograph (Fig. 6); 9a – number of fractures; 9b – total length of fractures; 9c – average length of fractures.

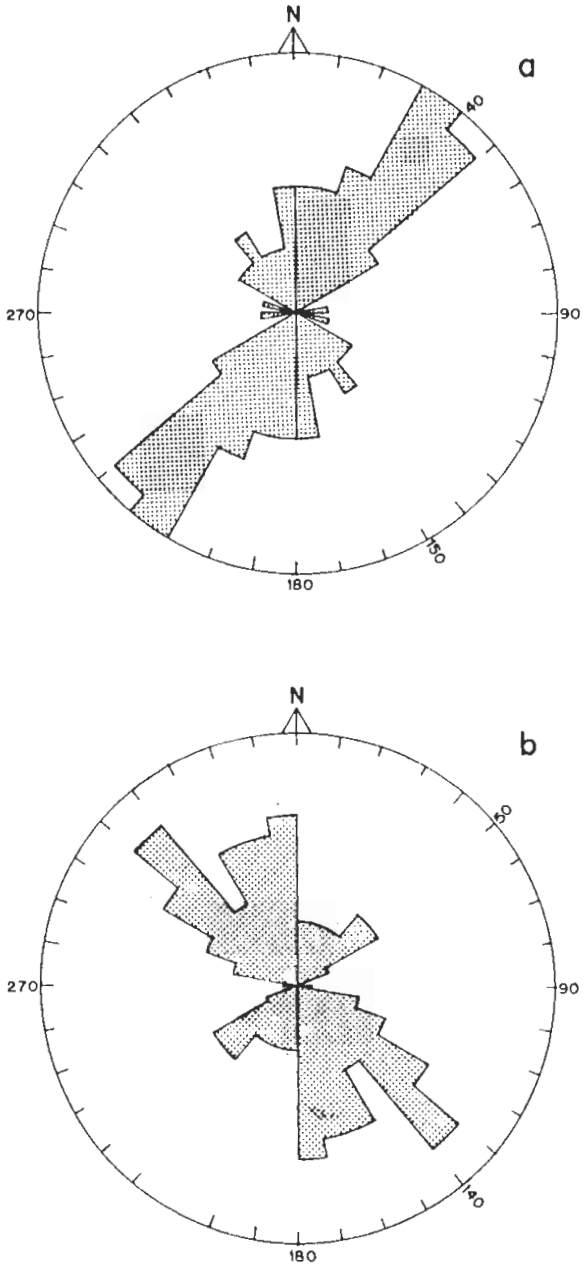

FIG. 10. Rose diagram for fractures measured in the field; 10a – fractures in the country rocks; 10b – fractures in the ring complex.

(1984) Fig. 11a, demonstrated that in rocks that were subjected to lateral EW compression a set of extensional fractures (1) develops in EW direction, a compressional set develops in NS direction (2) and a conjugated set of fractures develops in NE-SW (3) and in NW-SE (4).

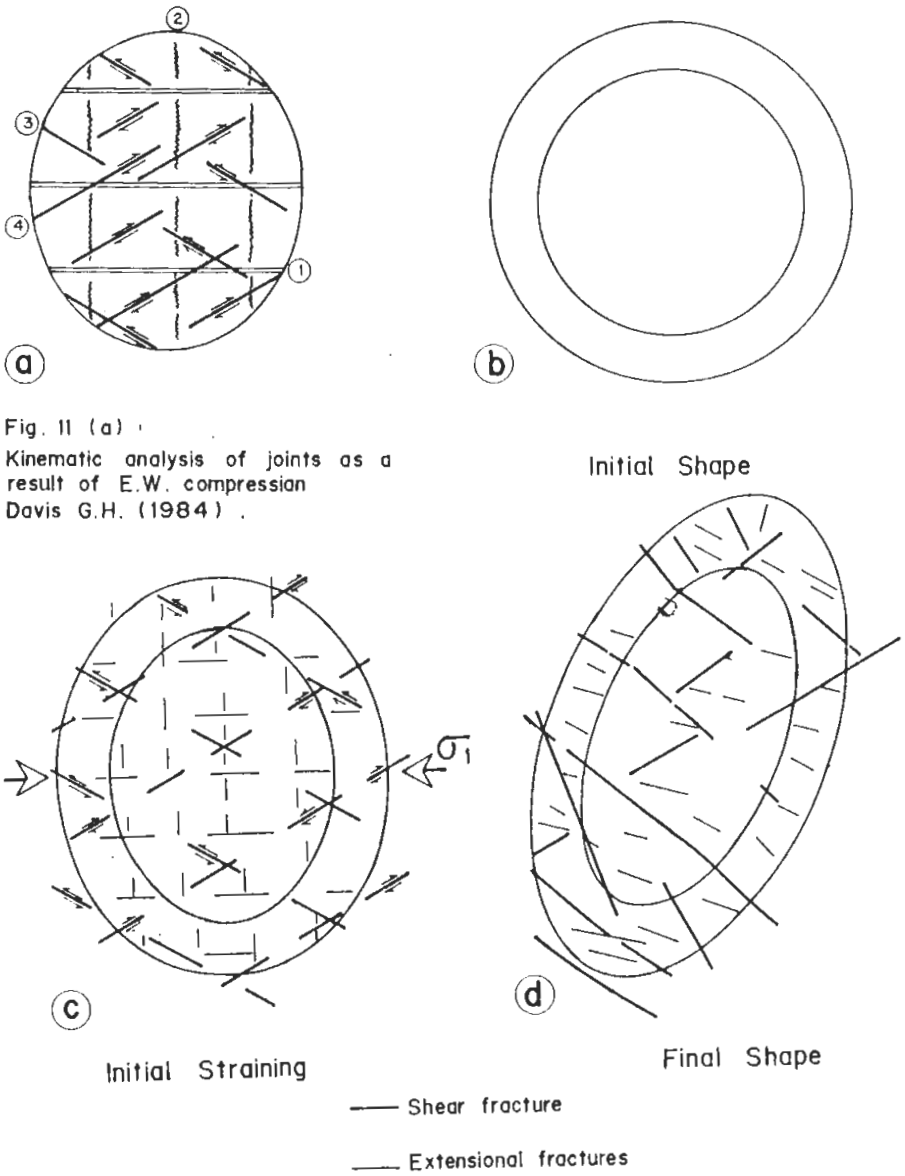

Fig. 11 (a) :
Kinematic analysis of joints as a result of E.W. compression
Davis G.H. (1984) .

FIG. 11. (a) Kinematic analysis of joints as a result of E-W compression Davis G.H. (1984).
(b,c,d) Stages in the development in the elleptical body and the associated lineaments.

A prominent set of NE trending shear fractures developed, together with some synthetic second order extensional fractures. First order ENE shear fractures developed to a lesser extent and accordingly their synthetic fractures are less common than those for the NE trend. However, as the deformation proceeded the angle between the NW-SE shear fractures and extensional E-W fractures become smaller, the body has apparently been rotated and some of the suggested sets of fractures were rarely visible.

The fracture or lineament pattern describes above (are illustrated by the various diagrams) correlates with the theoretical stress and strain model (Fig. 11). Therefore the fractures developed were diastrophic in nature.

The country rocks exhibited a more variable response to stress, due to their more complex tectonic history, as they were older than the ring complex.

TABLE 1. Frequencies of the number, total length average and length of fractures that are delineated from the Landsat Image, for each directional class.

Class Interval (degrees)	Frequency	Total Length (km)	Average Length (km)
0-9	8	36.1	3.9
10-19	1	6.1	6.1
20-29	7	4.0	4.0
30-39	3	2.5	2.5
40-49	8	3.4	3.4
50-59	9	2.1	2.1
60-69	6	2.0	2.0
70-79	8	3.9	3.9
80-89	1	3.1	3.1
90-99	5	8.2	8.1
100-109	2	3.7	3.7
110-119	5	5.1	5.1
120-129	2	13.0	13.0
130-139	4	10.5	10.5
140-149	5	7.7	7.7
150-159	12	58.9	4.9
160-169	8	5.0	5.0
170-179	3	4.7	4.7

Field Evaluation

Evaluation of Fractures

Field work was carried out to test the validity of conclusions on the fractures delineated from the satellite image (Fig. 4) and aerial photos (Fig. 7). The fractures that are weakly visible on the images needed careful field evaluation, but most could be observed. Obviously, many fractures in the field do not have any signature on the photos. In some instances, it was difficult to identify the fractures that were delineated from the images. There are many reasons for this discrepancy (e.g. dykes fil-

ling the fractures). Another difference is that sometimes, the fracture density is more intense in the field than can be deciphered from the images. However, it is concluded that most of the fractures that can be delineated from the images have field equivalents (Table 2, 3).

TABLE 2. Frequencies of the number, total length and average length of faults that are delineated from the aerial photos, for each directional class.

Class Interval	Frequency	Total Length (km)	Average Length (km)
0-9	0	0.000	0.000
10-19	0	0.000	0.000
20-29	0	0.000	0.000
30-39	0	0.000	0.000
40-49	0	0.000	0.000
50-59	0	0.000	0.000
60-69	0	0.000	0.000
70-79	0	0.000	0.000
80-89	1	9.692	9.692
90-99	2	19.316	9.658
100-109	3	8.122	2.707
110-119	2	11.930	5.965
120-129	6	27.317	4.553
130-139	9	51.542	5.727
140-149	2	12.693	6.347
150-159	1	9.741	9.741
160-169	2	8.451	4.225
170-179	1	9.546	9.546

TABLE 3. Frequencies of the number, total length and average length of fractures that are delineated from the Landsat Image, for each directional class.

Class Interval	Frequency	Total Length (km)	Average Length (km)
0-9	66	45.251	.686
10-19	57	40.070	.703
20-29	51	32.956	.646
30-39	31	19.789	.638
40-49	70	42.384	.605
50-59	68	46.289	.681
60-69	114	82.103	.720
70-79	123	91.337	.743
80-89	153	114.781	.750
90-99	190	130.808	.688
100-109	244	170.375	.698
110-119	320	215.646	.674
120-129	271	176.511	.651
130-139	184	118.150	.642
140-149	186	129.328	.695
150-159	156	110.979	.711
160-169	92	65.649	.714
170-179	83	57.026	.687

During the field work, the nature of fractures and their inter-relationships at outcrop scale were also investigated. In addition, fractures from both the ring complex and from the country rocks were studied.

The ring complex essentially contains two main fracture sets and one minor set. The main sets comprise one transverse to the long axis of the complex and one with a low angle attitude. The transverse fractures are very clearly expressed in the east where they form steep walled ridge trending NNE. The low angle set can be seen in the many parts of the complex (Pl. 2c). The minor set is approximately parallel to the NNE-SSW long axis of the elliptical complex.

Sometimes, one minor set of fractures (joints) is oblique to the associated major set (Pls. 2d and 2e), and the patterns of occurences of these two sets suggest some shearing, after one of the sets developed. In Plate (2d) the smaller fractures are slightly sigmoidal, and it can be suggested that the main fracture in the northern part of the plate could be a shear fracture.

Analysis

To understand the orientation relationships between fractures in the complex and those in the country rocks outside, separate rose diagrams were constructed (Figs. 10a and 10b). Figure 10a indicates clearly that the country rocks (felsic gneisses, mafic schists and mafic plutons) have fractures that are mostly oriented in a NE-SW direction. On the other hand, fractures within the ring complex have an essentially NW orientation, although they can be separated into two subsets; one striking NNW while the other is with a NE strike; there exists another minor set with a NE trend. Thus, a difference in the orientations of fractures within the complex and the country rocks, exist.

Discussion and Conclusion

During the present investigation, the fractures delineated from enhanced Landsat images are compared with those obtained from the aerial photographs. From this comparison for the Jabal Al-Hassir ring complex area, it can be concluded that although fractures delineated from the Landsat image closely correspond with those visible on the aerial photographs, the aerial photographs exhibit more details of the fracture system, because of their better resolution.

Field evaluation validated most of the fractures delineated from the Landsat image and aerial photos for the Jabal Al-Hassir area. As would be expected, many more fractures were found in the field than those delineated from the Landsat image and aerial photographs. This discrepancy is essentially related to the abundance of minor fractures and those that have very low or subhorizontal dips. It is concluded that, prior to any detailed field investigation, much of the fracture information can be obtained from the Landsat images and aerial photographs.

The discrepancy between the orientations of fracture systems in the ring complex and the country rocks, as identified during this study, aids modelling the tectonic

evolution of the Jabal Al-Hassir area in general, and the ring complex in particular (Divi *et al.* in preparation).

References

Anonymous (1982) *ARIES II Applications software package, version 2.00*, Operations Manual.

Coleman, R.G. (1972) Reconnaissance geology of the Khaybar Quadrangle, *Kingdom of Saudi Arabia. Dir. Gen. Min. Res., Kingdom of Saudi Arabia*, **GM-4.**

Davis, G.H. (1984) *Structural Geology of Rocks and Regions*, First ed., John Wiley and Sons.

Divi, S.R., Bahafazullah, H. and **Alwash, M.** *Structure and Petrology of the Jabal Al-Hassir area, Central Arabian Shield*, (in preparation).

Drysdall, A.R., Ramsay, C.R. and **Stoeser, D.B.** (1985) Felsic plutonic rocks and associated mineralization of the Kingdom of Saudi Arabia, Dyp. Ministry of Min. Res., Jeddah, *Min. Res. Resou. Bull.* **29.**

Johnson, P.R. and **Vranas, G.J.** (1984) The evolution of ideas concerning the stratigraphy and tectonic development of the Arabian Shield, *Dpy. Ministry of Min. Res., Open File Report.* **RF-OF-04-27,** 52 p.

Moore, G.K. and **Waltz, F.A.** (1983) Objectives procedures for lineament enhancement and extraction, *Photogrammetric Engineering and Remote Sensing*, **49** (5): 641-647.

Overstreet, W.C. (1978) A geologic and geotechnical reconnaissance of the Tathlith one-degree quadrangle, Sheet 19/43 Kingdom of Saudi Arabia, *Dir. Gen Min. Resour., Jeddah*, **SA(IR)-230,** 132 p.

Soha, J.M., Gillespie, A.R., Abrams, M.J. and **Madura, D.P.** (1976) Computer techniques for geologic applications, *in: CALTECH/JPL Symposium on Image Analysis Technology*, Pasodena, California, pp. 4-21.

Stacey, J.S. and **Hedge, C.E.** (1984) Geochronology and isotopic evidence for early Proterozoic continental crust in the eastern Arabian Shield, *Geology*, **12:** 310-313.

تحليل أنماط الكسور في المعقَّد الحلقي لجبل الحصير وسط الدرع العربي

محمد علي علوش و سار راو ديفي

كلية علوم الأرض ، جامعة الملك عبد العزيز ، جدة ، المملكة العربية السعودية

المستخلص . رُسمت الكسور من صور لاندسات المعززة والصور الجوية لمنطقة المعقد الحلقي لجبل الحصير بوسط الدرع العربي . ولقد تم التحقق من تلك الكسور في دراسة حقلية محددة وقياسات حقلية إضافية . وحللت الكسور المرسومة والصدوع المفسرة إحصائيا بأشكال التردد الدائرية بلغة الأرقام ، والطول الكلي ومتوسط طول الكسر لكل طائفة اتجاهية . وقورنت أنماط الكسور في المعقد الحلقي للقطع الناقص بأقرانها من الصخور المكتنفة . ويقترح تفسير التناقض بين هذين النمطين بأن مرده الاختلاف في التاريخ التكتوني للمعقَّد الحلقي والصخور المكتنفة المجاورة .